

Dynamic binding of RBPJ is determined by Notch signaling status

David Castel,^{2,3} Philippos Mourikis,^{2,3} Stefanie J.J. Bartels,^{1,3} Arie B. Brinkman,¹ Shahrugim Tajbakhsh,^{2,4} and Hendrik G. Stunnenberg^{1,4}

¹Department of Molecular Biology, Faculty of Science, Nijmegen Centre for Molecular Life Sciences, Radboud University Nijmegen, Nijmegen 6525 GA, the Netherlands; ²Stem Cells and Development, CNRS URA 2578, Department of Developmental and Stem Cell Biology, Institut Pasteur, 75015 Paris, France

Notch signaling plays crucial roles in mediating cell fate choices in all metazoans largely by specifying the transcriptional output of one cell in response to a neighboring cell. The DNA-binding protein RBPJ is the principle effector of this pathway in mammals and, together with the transcription factor moiety of Notch (NICD), regulates the expression of target genes. The prevalent view presumes that RBPJ statically occupies consensus binding sites while exchanging repressors for activators in response to NICD. We present the first specific RBPJ chromatin immunoprecipitation and high-throughput sequencing study in mammalian cells. To dissect the mode of transcriptional regulation by RBPJ and identify its direct targets, whole-genome binding profiles were generated for RBPJ; its coactivator, p300; NICD; and the histone H3 modifications H3 Lys 4 trimethylation (H3K4me3), H3 Lys 4 monomethylation (H3K4me1), and histone H3 Lys 27 acetylation (H3K27ac) in myogenic cells under active or inhibitory Notch signaling conditions. Our results demonstrate dynamic binding of RBPJ in response to Notch activation at essentially all sites co-occupied by NICD. Additionally, we identify a distinct set of sites where RBPJ recruits neither NICD nor p300 and binds DNA statically, irrespective of Notch activity. These findings significantly modify our views on how RBPJ and Notch signaling mediate their activities and consequently impact on cell fate decisions.

[**Keywords:** Rbpj; Notch; NICD; skeletal muscle; p300; ChIP-seq; RNA-seq]

Supplemental material is available for this article.

Received December 10, 2012; revised version accepted April 2, 2013.

Notch signaling influences a wide spectrum of stem and progenitor cell fate choices, and perturbations of this pathway lead to congenital defects, vascular disorders, and cancer (Gridley 2003; Louvi and Artavanis-Tsakonas 2012). Notch is a plasma membrane receptor, but its cleaved intracellular domain (NICD) is also a transcription factor (Greenwald 1985; Wharton et al. 1985; Schroeter et al. 1998). NICD interacts with RBPJ, a potent DNA-binding transcription factor that associates with a large number of chromatin regulators, corepressors, and coactivators (Jarriault et al. 1995; Kopan and Ilagan 2009). Analyzing the mode of transcriptional regulation by RBPJ and identifying its direct targets is fundamental for understanding how this transcription factor regulates diverse processes in response to Notch signaling but also independent of it.

To date, only a limited number of direct RBPJ-binding sites (enhancers and promoters) have been described.

Previous attempts to obtain a global view of RBPJ occupancies in mammalian cells by chromatin immunoprecipitation (ChIP) detected by sequencing (ChIP-seq) have been hindered by the lack of specific antibodies. Notably, a recent study performed on T-acute lymphoblastic leukemia cell lines (Wang et al. 2011) used a RBPJ antibody, which we now show to be inadequately characterized, as it cross-reacts with at least one other transcription factor, REST. Indeed, a large fraction of the proposed binding sites in those murine leukemic cells (32%) was highly enriched for the REST, but not the RBPJ, motif. In another ChIP-seq study (Li et al. 2012), RBPJ profiles were attempted from *in vivo* isolated murine neuronal cells of the cortex. However, the data show low depths of sequencing and a highly unusual distribution of reads for a transcription factor, with broad regions in the genome with low-definition peaks. More critically, the RBPJ-binding motif provided, based on the identified sites, is a degenerate 20-mer sequence that does not correspond to the consensus motif of this protein. These studies highlight the difficulties in obtaining meaningful genome-wide ChIP data for one of the most conserved signaling pathways.

³These authors contributed equally to this work.

⁴Corresponding authors

E-mail h.stunnenberg@ncmls.ru.nl

E-mail shaht@pasteur.fr

Article is online at <http://www.genesdev.org/cgi/doi/10.1101/gad.211912.112>.

To address the regulatory role of RBPJ, we conducted a genome-wide, temporal analysis of RBPJ binding by performing ChIP-seq in mammalian myogenic cells in the context of activated and repressed Notch signaling. We complemented this analysis with the identification of targets for NICD and the histone acetyltransferase (HAT) p300 (Ep300), which is a member of the RBPJ/NICD transcriptional activation complex (Oswald et al. 2001) and is associated with active enhancers (Visel et al. 2009). Moreover, we demonstrate that the vast majority of RBPJ-binding sites are in bona fide enhancers, featuring—in addition to p300—the hallmark modifications of histone H3 Lys 4 monomethylation (H3K4me1) and/or histone H3 Lys 27 acetylation (H3K27ac) (Fig. 1A). Significantly, we identified two distinct classes of binding sites. In the first class, RBPJ is dynamically recruited to its targets together with the cleaved intracellular domain

of Notch and p300. This inducible behavior of RBPJ controverts the classical view of static RBPJ binding to DNA (Barolo et al. 2002; Bray 2006), a view that was further reinforced recently in human T-cell lymphoblastic cells (Yatim et al. 2012). This dynamic property has been also attributed to Su(H) (fly RBPJ) for five enhancer elements of the *E(spl)* cluster (Krejci and Bray 2007) yet has not been clearly demonstrated in mammalian cells or on a whole-genome scale. In the second class, RBPJ is constitutively bound to DNA and unaffected by fluctuations of Notch activity. This class represents Notch-independent RBPJ regulatory elements, as they are not co-occupied by NICD in the cellular context studied.

In summary, our study constitutes the first specific genome-wide profile of RBPJ binding under different Notch activity conditions in mammalian cells. Our results provide a revised view on how RBPJ mediates Notch

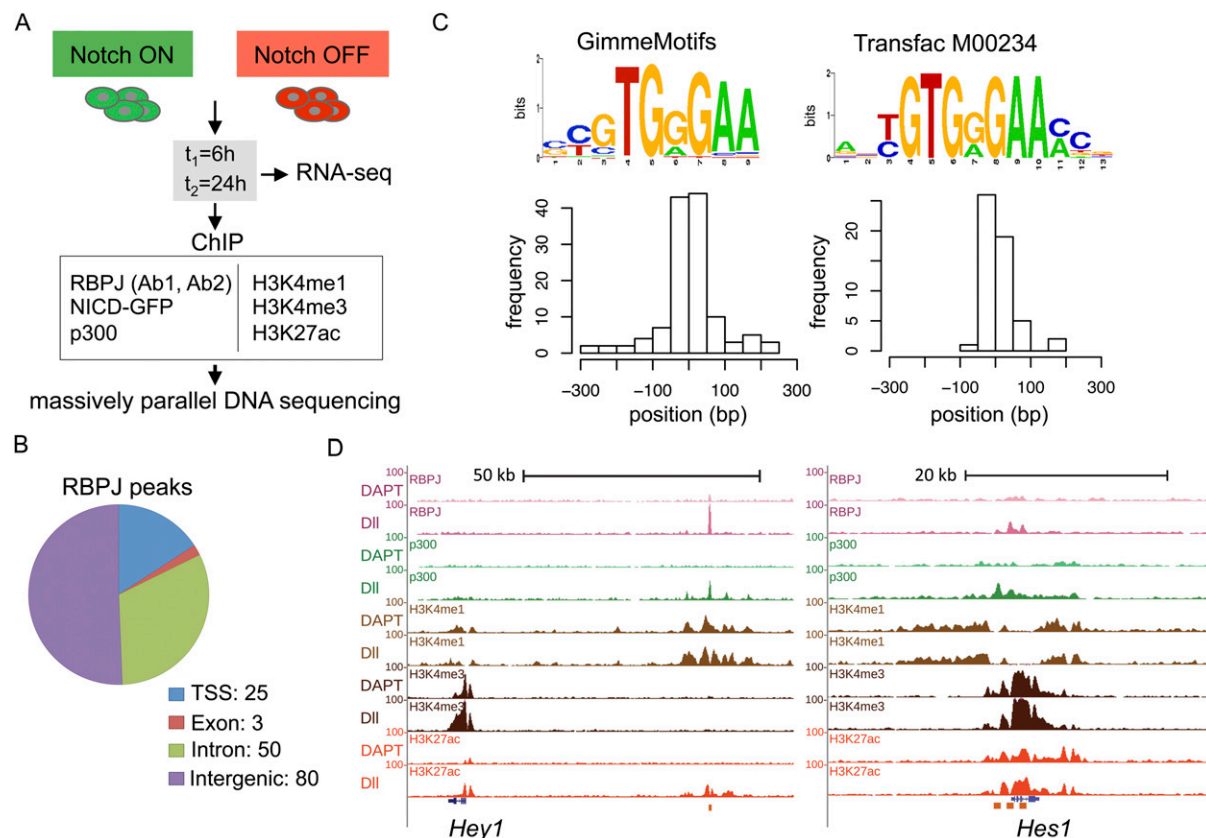


Figure 1. Genome-wide RBPJ-binding sites in mouse myogenic cells. (A) Notch signaling was activated or inhibited in myogenic C2C12 cells for different time intervals. Samples were subsequently processed for transcriptome analysis (RNA-seq) or ChIP and massively parallel DNA sequencing (ChIP-seq). ChIP was performed using two independent RBPJ antibodies (Ab1, monoclonal; Ab2, polyclonal), anti-p300, anti-GFP antibody for the NICD-GFP fusion, anti-H3K4me1, anti-H3K4me3, and H3K27ac. (B) Genomic distribution of RBPJ peaks (Ab1-RBPJ) in C2C12 cells. TSS regions were defined from 5 kb upstream of to 2 kb downstream from the TSS. (C) De novo motif search on the RBPJ peaks. (Left panel) Identified motif using GimmeMotifs; histogram displays the distribution of motif positions within the RBPJ peaks (0 is the peak summit as defined by the MACS peak-calling algorithm). (Right panel) RBPJ motif as present in the TRANSFAC database; histogram displays the distribution of motif positions detected with this matrix. (D) Examples of RBPJ-binding sites (pink) and p300-binding sites (green) and associated histone H3K4me1 (brown), H3K4me3 (dark brown), and H3K27ac (red) occupancy related to the known Notch pathway target genes *Hey1* and *Hes1*. Higher RBPJ binding accompanied by p300 can be observed in the cells cultured in the presence of the Notch ligand Dll1 as compared with DAPT. The orange box indicates RBPJ-binding position. See also Supplemental Figure S2A.

signaling activation to its target binding sites and challenge the notion of default repression as a global mechanism exerted by RBPJ in the absence of Notch signaling.

Results

RBPJ occupies a limited number of sites in mouse myogenic cells

To identify RBPJ-binding sites under different Notch signaling conditions, we performed ChIP-seq in mouse myogenic cells (C2C12) for targets of RBPJ and also of p300, a HAT that marks enhancer regulatory elements (Visel et al. 2009) and, together with NICD, acts as a coactivator of RBPJ (Oswald et al. 2001). We extended our analysis by generating chromatin state maps of H3K4me1, H3K27ac, and H3 Lys 4 trimethylation (H3K4me3) under activated or inhibited Notch signaling. The combination of these histone modifications contributed to a comprehensive characterization of the identified regulatory elements, as H3K27ac and p300 along with high H3K4me1 and low H3K4me3 constitute accurate markers of active enhancers, whereas high H3K4me3 together with low H3K4me1 mark proximal promoters (Heintzman et al. 2009; Creighton et al. 2010). Protein DNA binding and histone modifications were compared in cells either exposed to immobilized ligand Delta-like1 fused to Fc (Dll1-Fc) to activate the endogenous Notch receptors (Hicks et al. 2002) or treated with the γ -secretase inhibitor N-[N-(3,5-difluorophenacetyl)-L-alanyl]-S-phenylglycine t-butyl ester (DAPT) to block Notch signaling at different time intervals ($n = 2$) (Fig. 1A). Efficiency of induction by Dll1 and inhibition by DAPT were assessed by RT-qPCR (Supplemental Fig. S1A).

We used the model-based analysis of ChIP-seq (MACS) peak calling algorithm (Zhang et al. 2008) to identify RBPJ peaks in cells exposed to Dll1-Fc for 6 h (6 h, Dll1) versus input control. This yielded 158 RBPJ peaks. Of these, 78 RBPJ peaks (49%) were within or near genes (exonic, intronic, or -5 kb to $+2$ kb of transcription start sites [TSSs]), and 80 sites (51%) were intergenic (Fig. 1B). Of note, unlike a previous study (Wang et al. 2011), only a small fraction of RBPJ peaks (16%) was present near TSSs. De novo motif prediction in the 158 RBPJ peaks using GimmeMotifs (van Heeringen and Veenstra 2011) identified a highly enriched motif in 79% of all binding sites that corresponded to the known RBPJ-binding consensus (Fig. 1C). However, the RBPJ motif position weight matrix (PWM), as defined using our data set, differs slightly from that in TRANSFAC [Su(h), M00234], mainly in the nucleotide preferences flanking the conserved RBPJ hexameric motif TGG/AGAA (Fig. 1C; Supplemental Fig. S1B; Wingender 2008). In positional preference plots, RBPJ motifs were localized at the peak summits (Fig. 1C), indicating binding specificity of the RBPJ antibody (hereafter Ab1-RBPJ) used in ChIP-seq. Ab1-RBPJ specificity was further demonstrated by ChIP-qPCR by a loss of enrichment in *Rbpj*^{-/-} mouse embryonic fibroblasts (MEFs) (Supplemental Fig. S1C) and by indirect immunofluorescence (Supplemental Fig. S1D). We did not find

statistically significant enriched motifs for REST, CREB, and ETS, as previously described in mouse T-ALL RBPJ profiles (Wang et al. 2011), and PWM scan analysis corroborated this observation (Supplemental Fig. S1E).

We then analyzed RBPJ peaks for the presence of motifs located in tandem, as this has been proposed to lead to dimerization of RBPJ on DNA and subsequently favor transcriptional control (Nam et al. 2007). RBPJ motifs in tandem (GimmeMotifs matrix with cutoff 0.90 or 0.85) showed a preference for 11- to 21-base-pair (bp) spacing (Supplemental Fig. S1F). In addition, in 22 out of the 26 peaks containing the 11- to 21-bp spacer, the motifs were oriented head to head, as has been described for some RBPJ targets, including the archetypical target *Hes1* (Supplemental Table S1; Nam et al. 2007). Therefore, this head-to-head genomic arrangement is found only in a small fraction of total RBPJ-binding sites yet is a more likely configuration when more than one motif is present. RBPJ binding was observed adjacent to several known Notch targets, including *Hey1*, *Nrarp*, *Jagged1*, and *Hes1*, further validating our approach. Of note, with the exception of *Hes1*, the RBPJ peaks were not detected at the proximal promoters of these genes, but far away at presumed enhancer sites (at 50, 25, and 30 kb, respectively; all additional sites are available at Gene Expression Omnibus [GEO] no. GSE37184) (Fig. 1D for *Hey1* and *Hes1*).

Identification of inducible and constant RBPJ-binding sites in response to Notch signaling

Comparison of RBPJ occupancies in cells with activated or inhibited Notch signaling revealed a differential response to pathway activation. We observed that in most sites (95 out of 158), RBPJ binding was dynamic, with low or undetectable RBPJ occupancy in Notch-off cells and high occupancy in Notch-on cells (hereafter termed “inducible” sites). This pattern suggested enhanced binding to DNA of the activator RBPJ compared with the repressor RBPJ, a property described for Su(H) on five enhancer elements of the *E(spl)* genes cluster (Krejci and Bray 2007) but not comprehensively demonstrated in mammalian cells. The RBPJ site 50 kb upstream of the known NOTCH/RBPJ target and *E(spl)* homolog *Hey1* is representative of targets where RBPJ binding was greatly increased upon Notch activation (Fig. 1D). Similar inducible binding was observed on enhancers linked to novel RBPJ target genes (see Supplemental Fig. S2A for additional examples from 6-h and 24-h Dll1-treated or DAPT-treated samples). A unique mode of inducibility was observed for the platelet-derived growth factor receptor β (*Pdgfrb*), where the induced RBPJ binding 6 h after Notch activation (Fig. 2A) was reproducibly and strongly diminished after 24 h of exposure to the ligand (Supplemental Fig. S2A), representing a case of dynamic as well as temporal RBPJ binding. In the rest of the sites (63 out of 158), we observed constitutive RBPJ binding independent of Notch activity (hereafter termed “constant” sites). For example, the RBPJ-binding site between the *Krt9* and *Krt14* genes showed constant levels

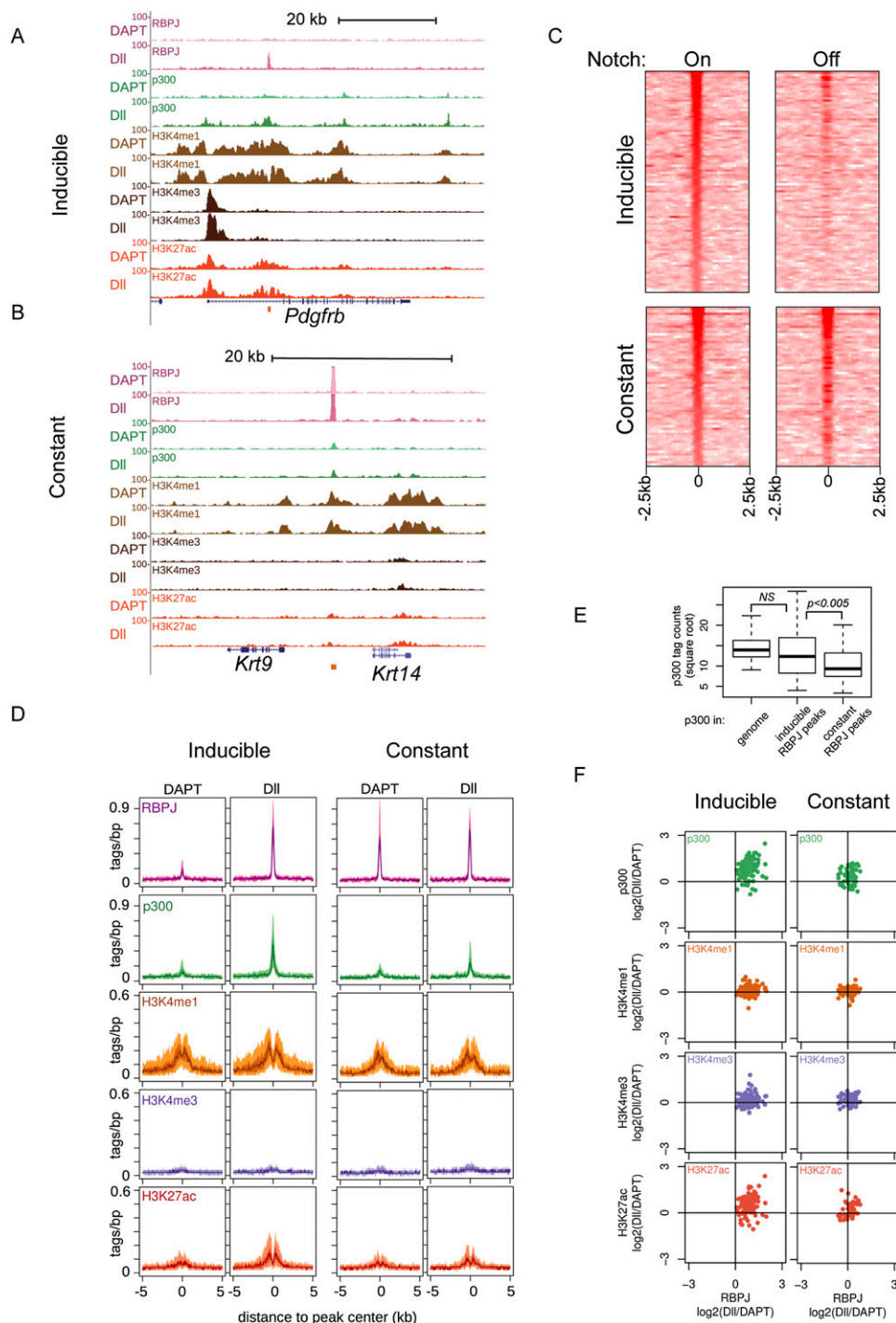


Figure 2. Identification of two classes of RBPJ-binding sites based on dynamic and static behavior in response to Notch activity. (A) Inducible RBPJ (pink) and p300 (green) binding and associated histone H3 modifications H3K4me1 (brown), H3K4me3 (dark brown), and H3K27ac (red) in response to 6 h of Dll1-Fc Notch activation in the first intron of the growth factor receptor *Pdgfrb*. See also Supplemental Figure S2A. (B) Constant RBPJ (pink) and p300 (green) binding and associated histone H3 modifications H3K4me1 (brown), H3K4me3 (dark brown), and H3K27ac (red) between the loci *Krt9* and *Krt14*. See also Supplemental Figure S2B. (C) Heat maps of RBPJ ChIP-seq read densities in inducible and constant sites from cells cultured for 6 h in the presence of Dll1-Fc (left) or Fc plus DAPT (right). Inducible peaks were defined by a decrease in tag counts to $\leq 60\%$ in DAPT compared with Dll1 conditions. Constant peaks were defined as peaks that maintained tag counts $>60\%$ in DAPT compared with Dll1. (D) ChIP-seq average profiles of RBPJ (pink), p300 (green), H3K4me1 (orange), H3K4me3 (blue), and H3K27ac (red) over inducible and constant RBPJ peaks under Notch-off (DAPT) or Notch-on (Dll) conditions. For each protein/histone modification, a three-color profile is used, showing the 25/75 percentile (lightest color), 40/60 percentile (intermediate color), and median (darkest color). (E) Box plot of p300 tag counts within all p300 peaks, inducible RBPJ sites, and constant RBPJ sites (derived from the ChIP-seq on 6-h Dll1-treated cells). p300 tag counts in constant sites are significantly lower than p300 tag counts in inducible sites; P -values were calculated using the Mann-Whitney U -test. (F) Scatter plots of $\log_2(\text{DII/DAPT})$ at 6 h of p300 (green), H3K4me1 (orange), H3K4me3 (blue), or H3K27ac (red) as a function of change in RBPJ occupancy for the inducible sites (left panel) and constant sites (right panel). Fold changes were calculated in windows of 2 kb centered over the RBPJ peaks. The accumulation in the top right quadrant indicates correlation between p300 or the different histone H3 modifications and RBPJ specifically at the inducible sites.

of RBPJ binding (Fig. 2B; see also Supplemental Fig. S2B for additional examples of constant sites).

The constant and inducible classes were clearly distinguishable in heat map representations (Fig. 2C) and average graphs, showing RBPJ ChIP-seq read densities at 6 h (Fig. 2D in pink) and 24 h (Supplemental Fig. S2C) after Dll1 or DAPT treatment. Similar results were obtained in replicate experiments (Supplemental Fig. S2D). Analysis of the inducible and constant sites separately did not reveal any specificity of motif, peak distribution, or tandem/head-to-head motifs (Supplemental Table S1; data not shown).

Notably, using an independent polyclonal RBPJ antiserum (hereafter Ab2-RBPJ) for ChIP-seq (Wang et al. 2011), similar results were obtained within the defined constant and inducible RBPJ sites, thereby corroborating the specificity of our analysis (Supplemental Fig. S3A,B). However, using Ab2-RBPJ, 388 additional sites were detected very highly enriched for the motif of the zinc finger transcription factor REST but not for the RBPJ motif (Supplemental Fig. S3C). The REST motif was also identified by a previous ChIP-seq study for RBPJ-binding sites in murine T-lymphoblastic leukemia cells using the Ab2-RBPJ antibody (Wang et al. 2011). The low enrichment of RBPJ motifs in these REST motif sites, as graphically demonstrated by ROC curves (receiver operator characteristic curves of sensitivity vs. specificity) (Supplemental Fig. S3D), prompted us to further investigate the specificity of this antibody. We performed ChIP-qPCR experiments with the Ab2-RBPJ antibody on wild-type and *Rbpj*-null MEFs (Kato et al. 1997) and found no signal loss at sites with a REST motif, demonstrating that the majority of the additional peaks were due to antibody cross-reactivity (Supplemental Fig. S3E). In contrast, we found specific loss of signal at all of the RBPJ sites (constant and inducible as defined by Ab1-RBPJ) (Supplemental Fig. S3F). Therefore, although Ab2-RBPJ cross-reacts with the transcription factor REST, it detects a small number of RBPJ peaks similar to that obtained in Ab1-RBPJ profiling. Taken together, our results using two different antibodies (Ab1, monoclonal; Ab2, polyclonal) demonstrate that the association of RBPJ to DNA is highly dynamic and strongly induced upon Notch signaling activation. However, at a subset of sites, RBPJ is constitutively bound to DNA.

To extend our analysis, we generated ChIP-seq profiles for the HAT p300 that is recruited to the core RBPJ/NICD complex by Mastermind-like proteins (Oswald et al. 2001; Fryer et al. 2002) and also marks active enhancers (Visel et al. 2009). To determine whether p300 recruitment can discriminate between inducible and constant RBPJ sites in the context of Notch-on and Notch-off states, we analyzed p300 ChIP-seq profiles from the same chromatin samples described above (6-h/24-h Dll1-Fc or Fc plus DAPT). We found that at the inducible sites, p300 behaved similarly to RBPJ, showing increased occupancies upon activation with Dll1 (Fig. 2A,B,D–F). At inducible sites, average RBPJ tag counts were higher for p300 than in constant sites, as demonstrated by the average tag densities (Fig. 2D–F). Interestingly, some constant sites contained p300 at levels similar to or even higher than the

inducible sites (Supplemental Fig. S2A [inducible peaks], B [constant peaks]). However, we note that in constant sites, modulations of Notch activity resulted in smaller p300 changes than in inducible sites, as shown by the scatter plots of Dll1/DAPT ratios for RBPJ versus p300 binding (Fig. 2F). Furthermore, Notch activation did not affect p300 occupancy (tag counts) at 10,207 peaks that did not overlap with either inducible or constant RBPJ sites (data not shown), thereby reinforcing the notion that the increase of p300 at inducible RBPJ peaks following Notch activation is highly significant and specific.

Chromatin signature of RBPJ-bound regulatory elements

The location of RBPJ-binding sites far away from promoters and the presence of the HAT p300 on the RBPJ-bound DNA elements (Fig. 2D) strongly suggested that these are active enhancers (Visel et al. 2009). As p300 is also a coactivator of the RBPJ/NICD complex (Oswald et al. 2001; Fryer et al. 2002), to unequivocally demonstrate that the RBPJ-bound elements are active enhancers, we generated whole-genome profiles of the global enhancer marks H3K4me1 and H3K27ac as well as of H3K4me3 that marks proximal promoters (Heintzman et al. 2009; Creighton et al. 2010). Profiles were produced for C2C12 cells exposed to Dll1 ligand or treated with DAPT to block Notch signaling. While H3K4me3 was largely absent, we found that RBPJ sites were enriched for H3K4me1 and H3K27ac. Interestingly, the H3K27ac was specifically increased at inducible RBPJ sites upon switching to Notch-activating conditions (Figs. 1D, 2A,B,D,F). The H3K27ac pattern at the distal *Hey1* enhancer constitutes a noteworthy example (Fig. 1D) where Notch activation induces de novo H3K27 acetylation, attributing a putative pioneering function to RBPJ. Taken together, our data demonstrate that the majority of the identified RBPJ-binding sites represent active enhancers, a subset of which is further activated upon Notch activation.

NICD is specifically recruited to inducible RBPJ-binding sites

The differential RBPJ occupancy and p300 recruitment upon Notch activation at static and dynamic sites suggested that RBPJ and the nuclear intracellular domain of Notch can also act autonomously of one another. To obtain a more comprehensive view of how Notch–RBPJ signaling operates, we determined NICD genomic occupancies in myogenic C2C12 cells and its association with inducible and constant RBPJ sites. Due to the lack of a reliable ChIP-grade Notch antibody, we used a tetracycline-inducible expression system to conditionally express the active intracellular fragment of Notch1 fused to GFP (NICD-GFP) or a GFP control protein. The functionality of the NICD-GFP fusion protein was validated by the induction of the target HEYL by Western blot analysis (Supplemental Fig. S4A). NICD and RBPJ genome-wide profiles were generated using anti-GFP and Ab1-RBPJ antibodies, respectively, on cells expressing NICD-GFP or GFP control 8 h after doxycycline induction (Fig. 3A).

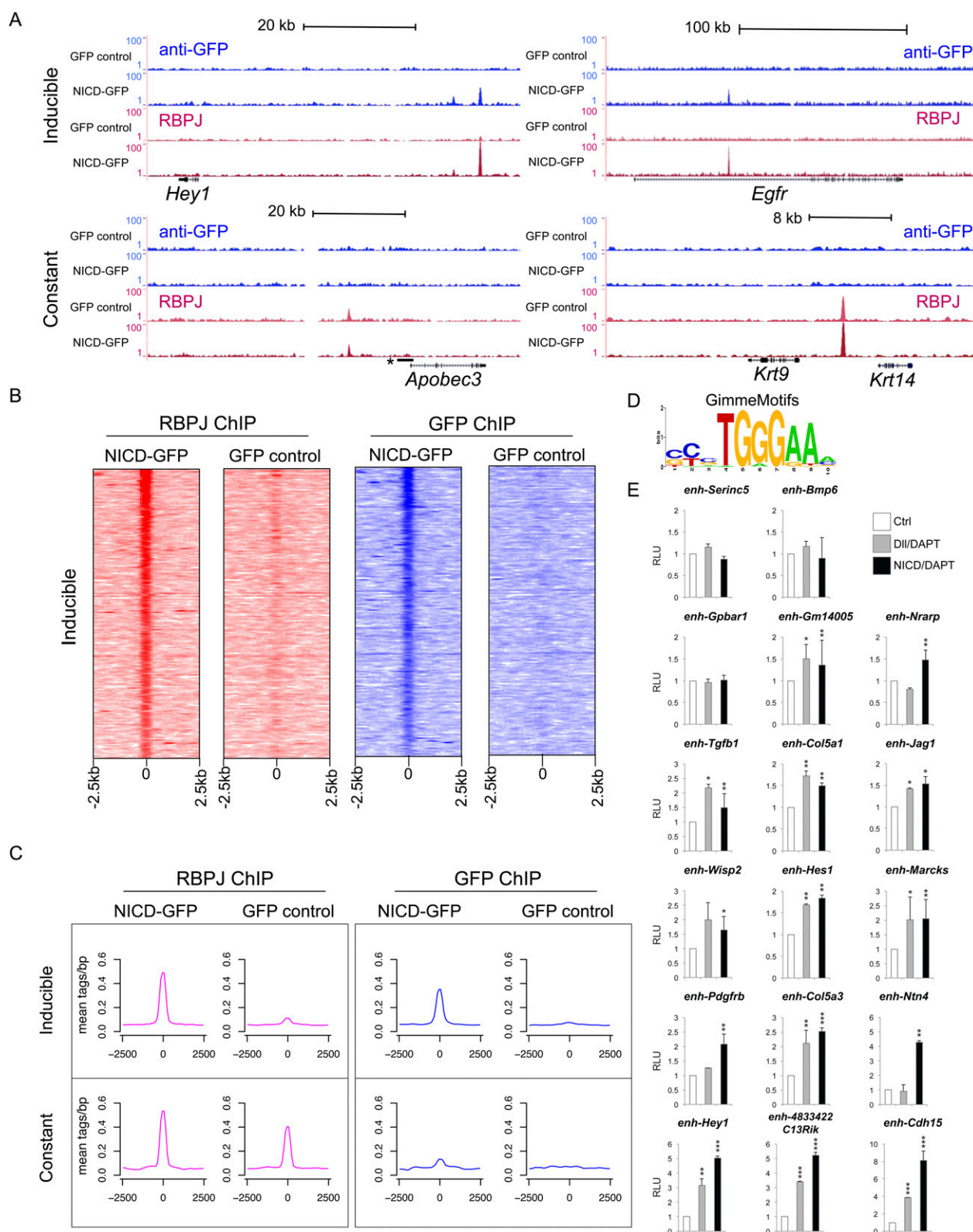


Figure 3. Inducible RBPJ sites, but not constant RBPJ sites, display NICD binding. (*A*, *top panel*) Examples of inducible RBPJ-binding sites displaying NICD-GFP cobinding. (*Bottom panel*) Examples of constant RBPJ-binding sites showing no NICD-GFP recruitment. Shown tracks were generated with an Ab1-RBPJ (pink) or anti-GFP (blue) antibody. Both antibodies were used for ChIP on GFP (control) and NICD-GFP-expressing cells. An asterisk indicates the predicted transcript *D730005E14Rik*. (*B*) Heat maps of RBPJ and GFP ChIP-seq read densities in the RBPJ/NICD-overlapping sites for the NICD-GFP- or GFP-expressing cells. (*C*) Average tag densities of anti-RBPJ (pink) and anti-GFP (blue) ChIP-seq in 5-kb regions around the inducible and constant sites for the various conditions. (*D*) PWM of the motif identified in the RBPJ/NICD-GFP-overlapping sites using GimmeMotifs. (*E*) Response of isolated enhancers to Notch signaling activation. Pathway activation was triggered by either Dll1-Fc (gray bars) or doxycycline-induced tetO-NICD-GFP (black bars). Relative luciferase signals are shown as ratios of Dll1-Fc over Fc+DAPT-treated cells \pm SD (gray bar, $n = 3$) or as ratios of NICD-GFP over GFP+DAPT \pm SD (black bars, $n = 3$). Firefly luciferase signals were normalized to pCMV-*Renilla*, and ratios were normalized to luciferase reporter minTK-Luciferase (white bar). Data are expressed as relative luminescence units (RLUs).

We performed MACS peak calling on both RBPJ and GFP tracks, combined the peaks, and analyzed RBPJ and NICD-GFP occupancies in Notch-on and Notch-off conditions. Out of 227 RBPJ sites, 211 showed inducible RBPJ binding (93%), and 16 sites showed constant RBPJ binding, as illustrated by heat maps of RBPJ read densities and average tag profiles (Fig. 3B,C). Interestingly, almost all inducible sites (94%) were also occupied by NICD, consistent with the recruitment of the NICD coactivator p300 in Dll1-induced cells (Fig. 2D), whereas none of the constant sites were occupied by NICD (Fig. 3B,C; Supplemental Fig. S4B). Individual examples of NICD-GFP occupancy at inducible and constant RBPJ sites are shown in Figure 3A. We note that in the NICD-GFP/GFP cells, we identified more inducible RBPJ sites than in the Dll1-induced cells (211 instead of 95, with 48 overlapping sites), whereas the number of constant RBPJ sites decreased from 63 to 16, with 12 sites overlapping between the two data sets. The larger number of inducible sites identified in the NICD-GFP compared with the Dll1-stimulated cells might be due to a more robust induction achieved with the NICD-GFP overexpression. We also note that 13 RBPJ peaks originally assigned as constant were all co-occupied by NICD and showed >60% increase in RBPJ occupancy upon NICD-GFP expression. Hence, these sites were classified as inducible in the NICD-GFP/GFP experiments. The overall increase in the number of inducible sites, however, does not originate from converting of constant to inducible sites; they comprise mainly new inducible sites. We speculate that these additional inducible sites represent lower-affinity sites that are manifested by the overexpression of NICD. Also, we note that several constant sites (25 out of 63) identified in the Dll1-induced C2C12 cells were not found in the cells overexpressing NICD. We propose that this could be due to a titration effect imposed by NICD overexpression, where RBPJ is sequestered away from other binding partners due to the high-affinity interaction between RBPJ and NICD (Del Bianco et al. 2008), as previously suggested (Kopan and Ilgan 2009).

De novo motif prediction on the RBPJ/NICD-overlapping sites identified the RBPJ motif with a PWM similar to that defined above (Fig. 3D). Using PWM scans, we found that all categories of RBPJ sites (inducible and constant) displayed high enrichments of the RBPJ motif (Supplemental Fig. S4C), corroborating the specificity of these RBPJ sites. Importantly, the average binding profiles of p300 and H3K27ac in the Dll1-stimulated cells were similar for the RBPJ sites exclusively identified in the NICD-GFP-expressing cells (Supplemental Fig. S4D,E). Thus, by using different tools to activate Notch signaling, we consistently identified inducible and constant RBPJ sites, thereby validating our observations.

Next, we tested the functionality of the novel NICD/RBPJ enhancers by measuring their activity in a cell-based luciferase assay. Seventeen candidate enhancers (Supplemental Table S2) were cloned in a luciferase construct upstream of the minimal thymidine kinase promoter (minTK-Luc) and introduced in C2C12 cells with active or inhibited Notch signaling. As shown in Figure 3E, the

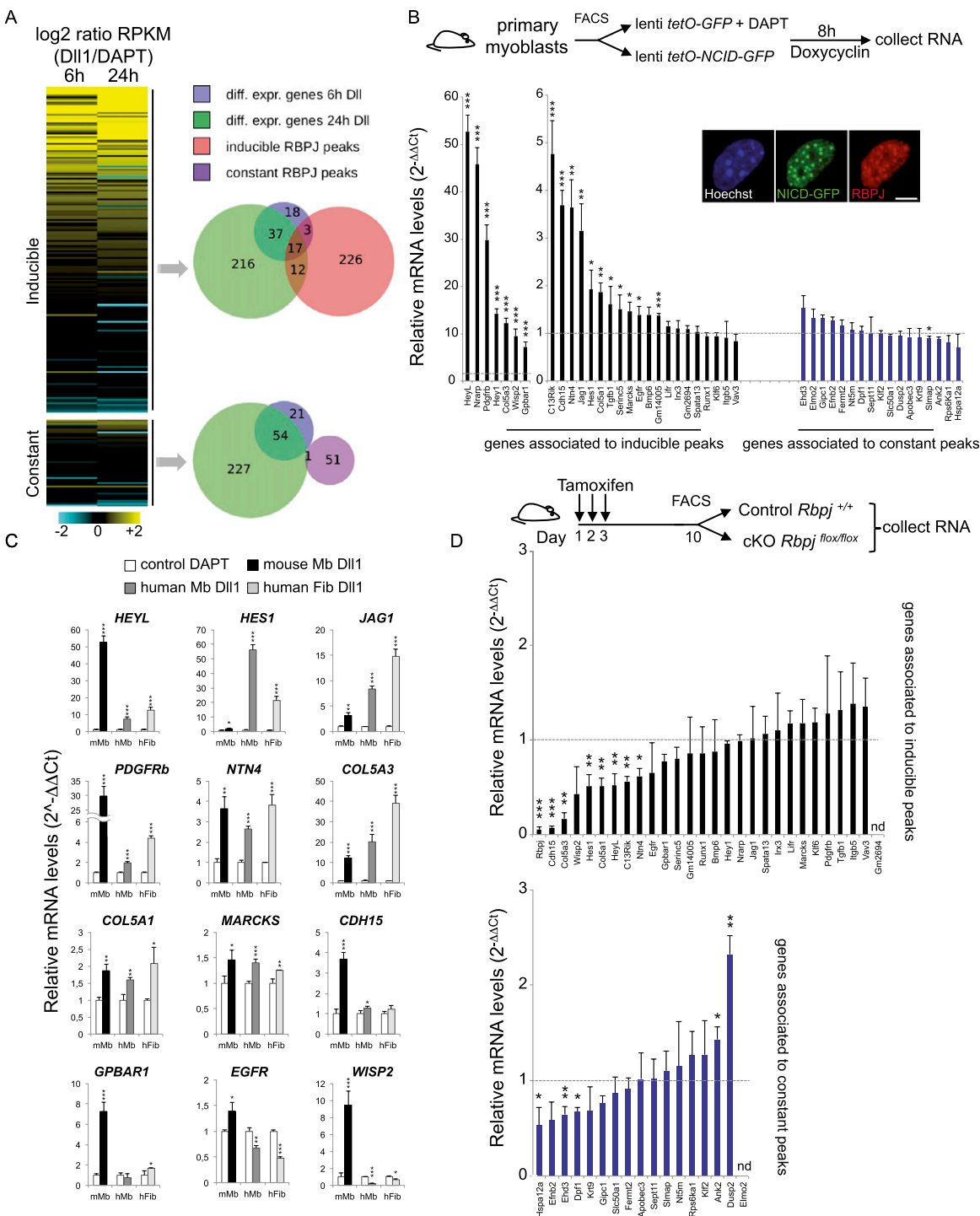
majority of the enhancers were induced upon Notch activation (10 of 17 enhancers with Dll1 and 14 of 17 with NICD activation) (Fig. 3E). Of note, a number of the enhancers tested conferred increased firefly luciferase activity compared with the minTK-Luc construct even in the presence of DAPT (data not shown). Therefore, some of the isolated elements appear to have enhancer activities independent of activated Notch.

Global transcriptional regulation by the NICD/RBPJ activator complex

The data presented above clearly demonstrate that the NICD/RBPJ transcriptional activator complex binds to a substantial number of functional enhancers that extend beyond the classical Hes/Hey targets. By extension, the profound impact of Notch signaling on muscle stem cell maintenance and differentiation is likely mediated by a broader number of direct targets than previously appreciated. To address this issue, we first compiled the peaks from the Ab1-RBPJ ChIP-seq experiments using both Dll1 and NICD-GFP activation (258 inducible and 52 constant peaks in total) (Supplemental Table S3) and performed an ontology analysis for the associated genes using GREAT (Genomic Regions Enrichment of Annotations Tool) (McLean et al. 2010). Analysis of the inducible RBPJ/NICD-binding sites reported enrichment for the Notch signaling pathway as well as for extracellular matrix components and cytokine/growth factor receptor binding (Supplemental Fig. S4F). In contrast, analysis on the constant sites did not give any significant enrichment.

Next, in order to determine the functional relevance of the RBPJ-binding sites to transcriptional regulation, we correlated them to genes that are differentially expressed between the Notch-on and Notch-off states. First, RNA-seq was performed on Dll1-stimulated C2C12 cells (6 h and 24 h), and DAPT-inhibited cells, and transcript levels were expressed as reads per kilobase of exon model per million mapped reads (RPKM). Pathway activation was validated by the up-regulation of known Notch targets in myogenic cells (*Hey1*, *HeyL*, *Nrarp*, and *Jag1*) (Supplemental Fig. S5A; Buas et al. 2009; Mourikis et al. 2012). Induction of the target genes in the C2C12 cells used is likely mediated by Notch-1, Notch-2, and Notch-3, but not Notch-4, as the latter is not expressed (average RPKMs of two experiments at 6 h/Dll1 were 10.6, 28.5, 13.8, and 0.07, respectively). Differential analysis was then performed using the DESeq package (Anders and Huber 2010), with a false discovery rate (FDR) at 0.05 and a twofold ratio threshold. We identified 55 induced and 20 repressed genes after 6 h of exposure to Dll1 and identified 115 induced and 167 repressed after 24 h exposure. In total, this represents 128 up-regulated and 175 down-regulated genes at either time point (Supplemental Table S4).

We then used the compiled list of peaks from the RBPJ ChIP-seq experiments (258 inducible and 52 constant peaks) and assigned them to the closest gene without a threshold on distance. The expression of these peak-associated genes was checked in the RNA-seq data, and average Dll1/DAPT expression ratios were visualized in a heat map (Fig. 4A).



Saturation analysis demonstrated that the RNA-seq depth was sufficient to identify all differentially expressed genes associated with RBPJ peaks (Supplemental Fig. S5B). We found that, out of the 190 expressed genes associated with inducible RBPJ peaks, 32 showed a significant up-regulation upon Notch activation (twofold or greater, $FDR \geq 0.05$) (Fig. 4A). In contrast, only one gene out of 51 linked to constant RBPJ sites was up-regulated. Consistently, up-regulation of these peak-related genes correlated to increased p300 and H3K27ac (Supplemental Fig. S5C). Of note, essentially no RBPJ peaks were associated to down-regulated genes. Therefore, the classification of the RBPJ sites into inducible and constant groups has a functional relevance, with the latter seemingly independent of Notch signaling in this cellular context (no NICD occupancy, no transcriptional induction).

Validation in primary myoblasts and Rbpj-null satellite cells

The transcriptional responses of target genes identified in C2C12 cells were also validated in primary myoblasts isolated by FACS from postnatal day 9 (P9) mice. Myoblasts were transduced with lentiviruses expressing either activated Notch (NICD-GFP) or GFP as a control, and the transcript levels were measured for selected targets by RT-qPCR (Fig. 4B). Significant up-regulation of the majority (66%) of the tested genes associated to inducible RBPJ sites was obtained by NICD overexpression, whereas the expression of the genes linked to constant RBPJ sites remained unaffected (Fig. 4B). Taken together, these results strongly suggest that the RBPJ binding that we identified in C2C12 cells is conserved in the primary cells. Furthermore, we tested some of the identified targets for conservation across species by activating Notch signaling in human myoblasts. In nine out of the 12 Notch targets tested, we found consistent transcriptional regulation in mouse and human myoblasts (Fig. 4C). Notably, in human myoblasts, unlike in the mouse, *HES1*, and not *HEYL*, was the most sensitive responder to pathway activation (Fig. 4C). Also, the induction of genes like *PDGFRb*, collagen *COL5A3*, and netrin *NTN4* was conserved between mice and humans, whereas *EGFR* and the WNT1-inducible signaling pathway protein 2 (*WISP2*) were not. Human skin fibroblasts were also used in the assay, and their induction was similar to those observed in the myogenic cells, indicating some degree of conservation also between different cell types (Fig. 4C).

To investigate in vivo the direct transcriptional regulation of the candidate target genes by RBPJ, we analyzed FACS-isolated adult muscle stem (satellite) cells in which *Rbpj* had been conditionally deleted and compared them with control cells (see the Materials and Methods). Satellite cells were selected for the loss-of-function studies, as Notch signaling is active in these cells and has been shown to be required for their maintenance (Bjornson et al. 2012; Mourikis et al. 2012). In cells lacking RBPJ protein, a significant number of genes associated to inducible peaks was down-regulated (seven of 27) (Fig. 4D).

Out of the 17 genes linked to constant RBPJ sites tested, three were significantly down-regulated in the *Rbpj*-null satellite cells (the heat-shock protein Hspa12a; the zinc finger transcription factor Dpf1; and Ehd3, a protein with a putative role in endocytic transport). Instead, ankyrin 2 (*Ank2*) and *Dusp2*, a phosphatase that negatively regulates MAP kinases, were up-regulated (Fig. 4D), suggesting that NICD-independent RBPJ may act as both an activator and a repressor in satellite cells.

Active repression by RBPJ does not occur on a subset of its targets

It has been shown that removal of RBPJ/Su(H) in the absence of NICD results in the transient activation (derepression) of some target genes (Morel and Schweisguth 2000; Koelzer and Klein 2003; Mulligan et al. 2011; Yatim et al. 2012). Our observation that RBPJ occupancy is strongly reduced at the inducible sites under Notch-off conditions prompted us to measure directly the repressive function of endogenous RBPJ in primary myogenic cells.

Quiescent satellite cells wild type or null for *Rbpj* were isolated by FACS and cultured in the presence of DAPT to prevent the formation of the RBPJ-activator complex (Fig. 5A). Two days after plating (on average, two to three cell divisions) (Rocheteau et al. 2012), cells were collected, and transcript levels were measured. We quantified the expression of 21 Notch-regulated genes associated with inducible RBPJ sites (Fig. 4B,D) and 17 genes associated with constant RBPJ sites. Ten out of 21 genes linked to inducible peaks showed derepression in the *Rbpj*-null cells, and 10 were not significantly affected (Fig. 5A). Notably, from the genes tested, only the expression of *M-cadherin* (*Cdh15*) was significantly reduced upon RBPJ withdrawal, suggesting that even in the absence of NICD, RBPJ mediates some level of activation on this locus. In contrast, among the 17 genes linked to constant RBPJ-binding sites, only *Dusp2* and *Ehd3* showed derepression upon depletion of the protein. Interestingly, *Dusp2* was also up-regulated in *Rbpj* knockout satellite cells, whereas *Ehd3* was down-regulated (Fig. 4D), indicating differential regulation of *Ehd3* in quiescent satellite cells (Notch-on) and in DAPT-treated primary myoblasts (Notch-off) (Fig. 5A). Our results therefore indicate that although RBPJ can act as both an activator and a repressor, on certain inducible sites, default RBPJ repression does not seem to occur.

Discussion

The CSL [CBF, RBPJ/Su(H)/Lag1] proteins are the only known transcription factors that mediate Notch signaling. The hitherto prevailing model purports that CSL proteins statically occupy gene regulatory sequences independent of the Notch signaling status and that upon activation of the pathway, NICD and other (co)activators are recruited to replace resident repressors. This model is compatible with the established property of CSL proteins as both transcriptional activators and repressors and, in a developmental context, with a mechanism to prevent

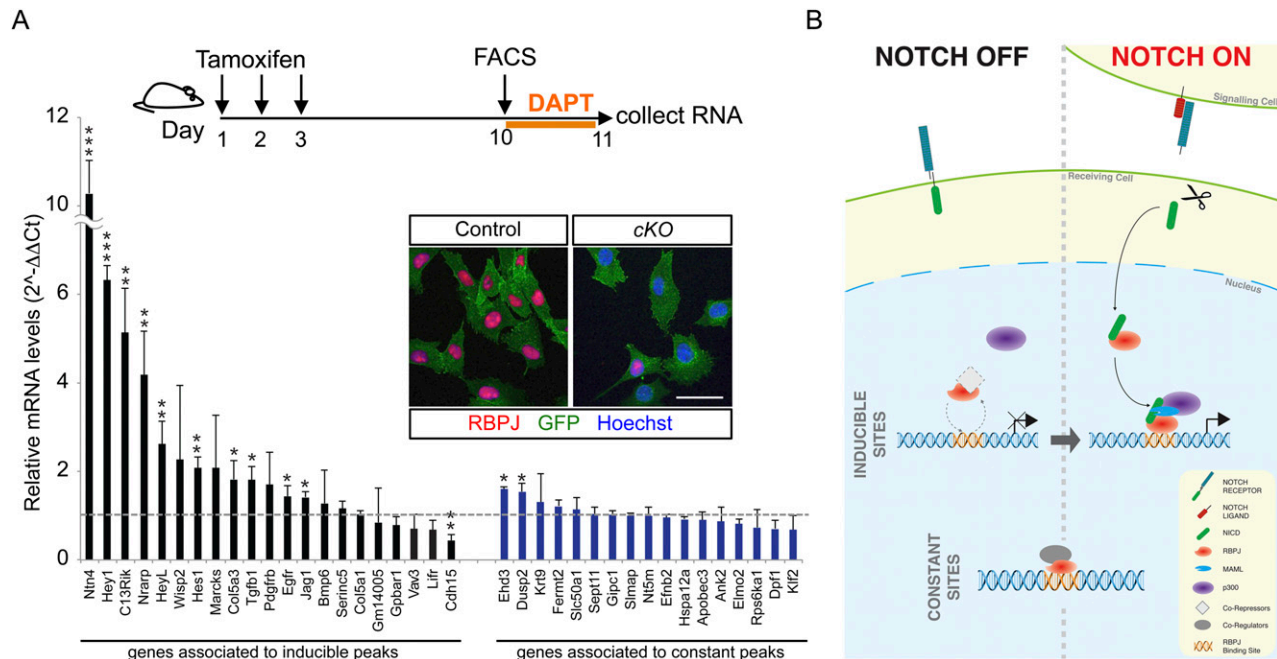


Figure 5. Release of active repression on a subset of RBPJ site-associated genes. (A) Transcript levels of target genes following depletion of RBPJ protein in the absence of Notch signaling. Control (*Tg:Pax7-CreERT2::Rbpj^{+/+}::R26^{mT/mG/+}*) and *Rbpj* conditional knockout (cKO) (*Tg:Pax7-CreERT2::Rbpj^{fllox/flox}::R26^{mT/mG/+}*) cells were FACS-purified and cultured in the presence of DAPT (orange bar on scheme). Histograms are ratios of normalized values of conditional knockout/control ($2^{-\Delta\Delta C_t} \pm SD$ ($n = 3$ mice per genotype)). (Inset on the right) Cultured myoblasts stained for RBPJ (Ab1; red) on the day of collection. The single red nucleus in the right panel is a recombination “escaper.” Transcript 4833422C13Rik was abbreviated to C13Rik. Bar, 25 μ m. (B) Inducible RBPJ-binding model in response to Notch signaling activation. Upon receptor activation and cleavage, the intracellular domain of Notch (NICD; green) translocates into the nucleus, where it binds RBPJ (red). We propose that NICD interacts with RBPJ off the DNA and subsequently is recruited to the “inducible” target sites to activate gene expression (black arrow). In the absence of NICD, RBPJ complexed with corepressors is weakly bound or not bound at all to DNA on those sites (dashed arrows). In contrast, NICD-independent RBPJ is statically bound to the “constant” sites, when Notch signaling activity is modulated. Constant sites contain the same RBPJ-binding motif as the inducible sites; hence, binding is likely to be specified by diverse partners (gray circle).

ectopic gene expression where Notch signaling is absent (default repression). Our data necessitate a reassessment of this model, demonstrating that RBPJ dynamically occupies essentially all identified NICD genomic targets, and, in certain cases, default repression is not taking place. Also, we identify a number of novel RBPJ target loci in muscle cells, several of which are independent of NICD and where RBPJ binding is static.

Using two different antibodies (Ab1, rat monoclonal, epitope not mapped; Ab2, rabbit polyclonal, amino acids 1–48 of hRBPJ), we unambiguously demonstrate that RBPJ dynamically binds DNA similar to the NICD activator itself. Isolated examples in the literature reported enhanced RBPJ binding on the promoters of *cyclin D3* and *Hes1* in mammalian cells following Notch pathway activation (Fryer et al. 2004; Joshi et al. 2009). In those studies, enriched RBPJ occupancies were shown by semiquantitative PCR analysis on chromatin-immunopurified material. Notably, for these ChIP experiments, two different polyclonal antibodies were used. In a more comprehensive study, regarding CSL dynamics, significant increase in Su(H) occupancy was scored on five regulatory elements of the *E(spl)* cluster following EDTA-induced Notch activation (Krejci and Bray 2007). Taken together,

these studies had challenged the static binding model of CSL proteins. Our results firmly establish these observations by demonstrating that dynamic RBPJ binding is the default mode of response to Notch activation across species.

Based on the revised model that we are reformulating on the basis of our genome-wide analysis, in the absence of Notch signaling, RBPJ binds weakly to enhancers and promoters targeted by NICD. In several cases, we noted that in DAPT-treated cells, RBPJ occupancy was decreased even below the levels of detection. This observation puts into question the repressive function of RBPJ at those sites. We addressed this question by scoring the release of target gene repression in the presence of DAPT in primary myoblasts in which RBPJ was conditionally removed genetically. We found that for some of the tested genes, removal of RBPJ function resulted in increased expression, suggesting that RBPJ indeed acts as a repressor even if it loosely binds DNA. However, for other Notch-regulated genes, RBPJ depletion did not up-regulate their expression, suggesting that under these experimental conditions, RBPJ is not exerting active repression.

Increased RBPJ occupancies at inducible sites following activation by Notch signaling suggest that RBPJ is

strongly recruited and/or binds more stably as part of the Notch-activating complex at these sites. Cooperative mechanisms are likely to play an important role in recruitment of RBPJ to its targets, introducing an additional level of gene target regulation by Notch. Which interactions are responsible for increased RBPJ-binding upon activation of Notch remains to be determined. It must be noted that only a small fraction of sites contains paired motifs, and thus cooperative assembly of dimeric Notch complexes is unlikely to be the mechanism behind inducible binding.

Given the discrepancies in phenotypes between *Notch*- and *Rbpj*-null mutants (Tanigaki and Honjo 2010), it has been postulated that these factors might also function independently. To date, only an atypical RBPJ/PTF1A activation complex that does not contain NICD has been described during the generation of GABAergic neurons (Hori et al. 2008). Our study uncovers a distinct set of RBPJ-binding sites that are not co-occupied by NICD. The nature of the binding partners of RBPJ and the extent to which they are conserved among these sites have not been investigated. Furthermore, the functional significance of these sites and the genes that they associate with also remains unknown.

Our findings lead us to propose that inducible and constant RBPJ peaks do not represent two distinct ways to respond to NICD, but rather the existence of Notch-dependent and Notch-independent complexes. These findings modify significantly our current understanding of how RBPJ, in conjunction with Notch signaling, regulates gene expression in muscle cells and consequently how this impacts on cell fate decisions during myogenesis. Future work will show whether RBPJ dynamics define a general phenomenon during the transduction of Notch signaling.

Materials and methods

ChIP-seq

Chromatin harvesting and ChIP experiments were performed as described by Denisov et al. (2007) and in GEO no. GSE37184. The following antibodies were used: rat monoclonal anti-RBPJ antibody clone 1F1 (Ab1) (provided by E. Kremmer via Ascenion) (Ehm et al. 2010), rabbit polyclonal anti-RBPJ (Ab2) (kindly provided by E. Kieff and collaborators) (Wang et al. 2011; Zhao et al. 2011), rabbit polyclonal anti-p300 antibody C-20 (sc-585, Santa Cruz Biotechnology) (Visel et al. 2009), and goat polyclonal anti-GFP antibody (kindly provided by M. Vermeulen). ChIP DNA was prepared for Illumina sequencing according to the manufacturer's protocols (Illumina) or used for ChIP-qPCR assay. DNA was prepared for Illumina sequencing according to the manufacturer's protocols (Illumina) or used for ChIP-qPCR assay. A detailed protocol of the ChIP-seq of histone modifications is described in the Supplemental Material. ChIP-seq samples, antibodies used, and number of reads per sample are described in Supplemental Table S5.

RNA-seq (strand-specific)

Total RNA was extracted using RNeasy minikit and microkit (Qiagen) following the manufacturer's instructions. Ribosomal

RNA was removed from 200 ng of total RNA using the Ribo-Zero rRNA Removal kit Low Input for Human/Mouse/Rat (Epicentre Biotechnologies) according to the manufacturer's protocol. RNA was subsequently fragmented in fragmentation buffer (40 mM Tris-Ac at pH 8.2, 100 mM KAc, 30 mM MgAc) for 90 sec at 95°C and purified by ethanol purification. cDNA was synthesized using random hexamers by SuperScript III reverse transcriptase (Invitrogen) in the presence of 6 ng/ μ L ActinomycinD. cDNA was purified (MinElute Reaction Cleanup kit, Qiagen) and subjected to second strand synthesis by *Escherichia coli* DNA polymerase I (Invitrogen) and *E. coli* DNA ligase (New England Biolabs) in the presence of RNase H (Ambion). For second strand synthesis, dUTPs were used containing dUTP instead of dTTP. ds-cDNA was purified (MinElute Reaction Cleanup kit, Qiagen) and prepared for Illumina sequencing according to standard procedures. Before final PCR amplification, uracil containing second strand DNA was removed by USER enzyme (New England Biolabs) for 15 min at 37°C followed by 10 min at 95°C in 1 \times Phusion buffer (Finnzymes). RNA-seq samples and number of reads per sample are described in Supplemental Table S5.

Detection of differentially expressed genes

To detect differentially expressed genes, we used a model based on the negative binomial distribution of all RefSeq genes, as available in the DESeq package (Anders and Huber 2010). To account for biological variability, two biological replicates for each condition were used. A fold difference of at least two and an FDR <0.05 were used as cutoffs to identify differentially expressed genes.

Bioinformatics analyses

RBPJ, p300, and NICD peaks were called by MACS (version 1.4.Orc2) (Zhang et al. 2008) with $P = 1 \times 10^{-8}$ and $mfold = 5$ and an input control. Inducible peaks were defined by a decrease in tag counts to $\leq 60\%$ in DAPT compared with Dll1 conditions. Constant peaks were defined as peaks that maintained tag counts $>60\%$ in DAPT compared with Dll1. GimmeMotifs was used for de novo motif prediction using default settings (van Heeringen and Veenstra 2011). Motif occurrences were determined by PWM scans with cutoff 0.9. For calculation of motif enrichments over background, a set of random genomic sequences with a genomic distribution similar those of the peak sequences was used. Further data analyses were performed in LINUX shell, Python, Perl, and R, using in-house-generated scripts. Gene annotations were based on RefSeq (mm9).

Quantitative PCR and ChIP-qPCR

Quantitative PCR was performed using SYBR Green-based mix (Invitrogen), and analysis was performed using the $2^{-\Delta\Delta CT}$ method (Livak and Schmittgen 2001). Primers used in this study are listed in Supplemental Table S6.

Statistical analysis of primary cell samples

For comparison between two groups, two-tailed Student's *t*-test was performed to calculate *P*-values and determine statistically significant differences ([*] $P < 0.05$; [**] $P < 0.01$; [***] $P < 0.001$). All statistical analyses were performed with Excel software.

Acknowledgments

We are indebted to E. Janssen-Megens, Y. Tan, K.J. François, and H. Kerstens for technical support. We thank S. van Heeringen for

extensive help with motif analyses. We also thank the platform for immortalization of human cells of the Myology Institute in Paris and V. Allamand for immortalized human myoblasts and primary fibroblasts, respectively; U. Lendahl for NICD1-GFP; and E. Kieff for polyclonal anti-RBPJ. We acknowledge the Plate-Forme de Cytométrie (PFC, Institut Pasteur, Paris) and especially P-H. Commere. We thank E. Kremmer and M. Vermeulen for kindly providing anti-RBPJ and anti-GFP antibodies, respectively. We also acknowledge support from the Institut Pasteur; Association Française Contre les Myopathies; Agence Nationale de la Recherche (ANR-06-BLAN-0039; and Revive, Investissement d'Avenir, ANR-10-LABX-73); Association pour la Recherche sur le Cancer; EU Framework 7 projects EuroSystem, Optistem, and NotchIT; and the Fondation pour la Recherche Médicale.

References

- Anders S, Huber W. 2010. Differential expression analysis for sequence count data. *Genome Biol* **11**: R106.
- Barolo S, Stone T, Bang AG, Posakony JW. 2002. Default repression and Notch signaling: Hairless acts as an adaptor to recruit the corepressors Groucho and dCtBP to Suppressor of Hairless. *Genes Dev* **16**: 1964–1976.
- Bjornson CR, Cheung TH, Liu L, Tripathi PV, Steeper KM, Rando TA. 2012. Notch signaling is necessary to maintain quiescence in adult muscle stem cells. *Stem Cells* **30**: 232–242.
- Bray SJ. 2006. Notch signalling: A simple pathway becomes complex. *Nat Rev Mol Cell Biol* **7**: 678–689.
- Buas ME, Kabak S, Kadesch T. 2009. Inhibition of myogenesis by Notch: Evidence for multiple pathways. *J Cell Physiol* **218**: 84–93.
- Creyghton MP, Cheng AW, Welstead GG, Kooistra T, Carey BW, Steine EJ, Hanna J, Lodato MA, Frampton GM, Sharp PA, et al. 2010. Histone H3K27ac separates active from poised enhancers and predicts developmental state. *Proc Natl Acad Sci* **107**: 21931–21936.
- Del Bianco C, Aster JC, Blacklow SC. 2008. Mutational and energetic studies of Notch 1 transcription complexes. *J Mol Biol* **376**: 131–140.
- Denissov S, van Driel M, Voit R, Hekkelman M, Hulsen T, Hernandez N, Grummt I, Wehrens R, Stunnenberg H. 2007. Identification of novel functional TBP-binding sites and general factor repertoires. *EMBO J* **26**: 944–954.
- Ehm O, Goritz C, Covic M, Schaffner I, Schwarz TJ, Karaca E, Kempkes B, Kremmer E, Pfeieger FW, Espinosa L, et al. 2010. RBPJ κ -dependent signaling is essential for long-term maintenance of neural stem cells in the adult hippocampus. *J Neurosci* **30**: 13794–13807.
- Fryer CJ, Lamar E, Turbachova I, Kintner C, Jones KA. 2002. Mastermind mediates chromatin-specific transcription and turnover of the Notch enhancer complex. *Genes Dev* **16**: 1397–1411.
- Fryer CJ, White JB, Jones KA. 2004. Mastermind recruits CycC:CDK8 to phosphorylate the Notch ICD and coordinate activation with turnover. *Mol Cell* **16**: 509–520.
- Greenwald I. 1985. *lin-12*, a nematode homeotic gene, is homologous to a set of mammalian proteins that includes epidermal growth factor. *Cell* **43**: 583–590.
- Gridley T. 2003. Notch signaling and inherited disease syndromes. *Hum Mol Genet* **12**: R9–R13.
- Heintzman ND, Hon GC, Hawkins RD, Kheradpour P, Stark A, Harp LF, Ye Z, Lee LK, Stuart RK, Ching CW, et al. 2009. Histone modifications at human enhancers reflect global cell-type-specific gene expression. *Nature* **459**: 108–112.
- Hicks C, Ladi E, Lindsell C, Hsieh JJ, Hayward SD, Collazo A, Weinmaster G. 2002. A secreted Delta1-Fc fusion protein functions both as an activator and inhibitor of Notch1 signaling. *J Neurosci Res* **68**: 655–667.
- Hori K, Cholewa-Waclaw J, Nakada Y, Glasgow SM, Masui T, Henke RM, Wildner H, Martarelli B, Beres TM, Epstein JA, et al. 2008. A nonclassical bHLH Rbpj transcription factor complex is required for specification of GABAergic neurons independent of Notch signaling. *Genes Dev* **22**: 166–178.
- Jarriault S, Brou C, Logeat F, Schroeter EH, Kopan R, Israel A. 1995. Signalling downstream of activated mammalian Notch. *Nature* **377**: 355–358.
- Joshi I, Minter LM, Telfer J, Demarest RM, Capobianco AJ, Aster JC, Sicinski P, Fauq A, Golde TE, Osborne BA. 2009. Notch signaling mediates G1/S cell-cycle progression in T cells via cyclin D3 and its dependent kinases. *Blood* **113**: 1689–1698.
- Kato H, Taniguchi Y, Kurooka H, Minoguchi S, Sakai T, Nomura-Okazaki S, Tamura K, Honjo T. 1997. Involvement of RBP-J in biological functions of mouse Notch1 and its derivatives. *Development* **124**: 4133–4141.
- Koelzer S, Klein T. 2003. A Notch-independent function of Suppressor of Hairless during the development of the bristle sensory organ precursor cell of *Drosophila*. *Development* **130**: 1973–1988.
- Kopan R, Ilagan MX. 2009. The canonical Notch signaling pathway: Unfolding the activation mechanism. *Cell* **137**: 216–233.
- Krejci A, Bray S. 2007. Notch activation stimulates transient and selective binding of Su(H)/CSL to target enhancers. *Genes Dev* **21**: 1322–1327.
- Li Y, Hibbs MA, Gard AL, Shylo NA, Yun K. 2012. Genome-wide analysis of N1ICD/RBPJ targets in vivo reveals direct transcriptional regulation of Wnt, SHH, and hippo pathway effectors by Notch1. *Stem Cells* **30**: 741–752.
- Livak KJ, Schmittgen TD. 2001. Analysis of relative gene expression data using real-time quantitative PCR and the $2^{-\Delta\Delta C_T}$ method. *Methods* **25**: 402–408.
- Louvi A, Artavanis-Tsakonas S. 2012. Notch and disease: A growing field. *Semin Cell Dev Biol* **23**: 473–480.
- McLean CY, Bristol D, Hiller M, Clarke SL, Schaar BT, Lowe CB, Wenger AM, Bejerano G. 2010. GREAT improves functional interpretation of cis-regulatory regions. *Nat Biotechnol* **28**: 495–501.
- Morel V, Schweisguth F. 2000. Repression by suppressor of hairless and activation by Notch are required to define a single row of single-minded expressing cells in the *Drosophila* embryo. *Genes Dev* **14**: 377–388.
- Mourikis P, Sambasivan R, Castel D, Rocheteau P, Bizzarro V, Tajbakhsh S. 2012. A critical requirement for notch signaling in maintenance of the quiescent skeletal muscle stem cell state. *Stem Cells* **30**: 243–252.
- Mulligan P, Yang F, Di Stefano L, Ji JY, Ouyang J, Nishikawa JL, Toiber D, Kulkarni M, Wang Q, Najafi-Shoushtari SH, et al. 2011. A SIRT1–LSD1 corepressor complex regulates Notch target gene expression and development. *Mol Cell* **42**: 689–699.
- Nam Y, Sliz P, Pear WS, Aster JC, Blacklow SC. 2007. Cooperative assembly of higher-order Notch complexes functions as a switch to induce transcription. *Proc Natl Acad Sci* **104**: 2103–2108.
- Oswald F, Tauber B, Dobner T, Bourteelle S, Kostezka U, Adler G, Liptay S, Schmid RM. 2001. p300 acts as a transcriptional coactivator for mammalian Notch-1. *Mol Cell Biol* **21**: 7761–7774.
- Rocheteau P, Gayraud-Morel B, Siegl-Cachedenier I, Blasco MA, Tajbakhsh S. 2012. A subpopulation of adult skeletal muscle stem cells retains all template DNA strands after cell division. *Cell* **148**: 112–125.
- Schroeter EH, Kisslinger JA, Kopan R. 1998. Notch-1 signalling requires ligand-induced proteolytic release of intracellular domain. *Nature* **393**: 382–386.

- Tanigaki K, Honjo T. 2010. Two opposing roles of RBP-J in Notch signaling. *Curr Top Dev Biol* **92**: 231–252.
- van Heeringen SJ, Veenstra GJ. 2011. GimmeMotifs: A de novo motif prediction pipeline for ChIP-sequencing experiments. *Bioinformatics* **27**: 270–271.
- Visel A, Blow MJ, Li Z, Zhang T, Akiyama JA, Holt A, Plajzer-Frick I, Shoukry M, Wright C, Chen F, et al. 2009. ChIP-seq accurately predicts tissue-specific activity of enhancers. *Nature* **457**: 854–858.
- Wang H, Zou J, Zhao B, Johannsen E, Ashworth T, Wong H, Pear WS, Schug J, Blacklow SC, Arnett KL, et al. 2011. Genome-wide analysis reveals conserved and divergent features of Notch1/RBPJ binding in human and murine T-lymphoblastic leukemia cells. *Proc Natl Acad Sci* **108**: 14908–14913.
- Wharton KA, Johansen KM, Xu T, Artavanis-Tsakonas S. 1985. Nucleotide sequence from the neurogenic locus notch implies a gene product that shares homology with proteins containing EGF-like repeats. *Cell* **43**: 567–581.
- Wingender E. 2008. The TRANSFAC project as an example of framework technology that supports the analysis of genomic regulation. *Brief Bioinform* **9**: 326–332.
- Yatim A, Benne C, Sobhian B, Laurent-Chabalier S, Deas O, Judde JG, Lelievre JD, Levy Y, Benkirane M. 2012. NOTCH1 nuclear interactome reveals key regulators of its transcriptional activity and oncogenic function. *Mol Cell* **48**: 445–458.
- Zhang Y, Liu T, Meyer CA, Eeckhoutte J, Johnson DS, Bernstein BE, Nusbaum C, Myers RM, Brown M, Li W, et al. 2008. Model-based analysis of ChIP-seq (MACS). *Genome Biol* **9**: R137.
- Zhao B, Zou J, Wang H, Johannsen E, Peng CW, Quackenbush J, Mar JC, Morton CC, Freedman ML, Blacklow SC, et al. 2011. Epstein-Barr virus exploits intrinsic B-lymphocyte transcription programs to achieve immortal cell growth. *Proc Natl Acad Sci* **108**: 14902–14907.

Erratum

Genes & Development 27: 1059–1071 (2013)

Dynamic binding of RBPJ is determined by Notch signaling status

David Castel, Philippos Mourikis, Stefanie J.J. Bartels, Arie B. Brinkman, Shahragim Tajbakhsh, and Hendrik G. Stunnenberg

For the above-mentioned article, in the right panel of the Supplemental Figure S1D, blue nuclei and the “Hoechst” text below it appeared erroneously in pink. In addition, panels A and B were missing from the originally published Supplemental Figure S2. These issues have been corrected in the Revised Supplemental file online: Revised_SuppFigs_S1_S2.pdf.



Dynamic binding of RBPJ is determined by Notch signaling status

David Castel, Philippos Mourikis, Stefanie J.J. Bartels, et al.

Genes Dev. 2013, **27**:

Access the most recent version at doi:[10.1101/gad.211912.112](https://doi.org/10.1101/gad.211912.112)

Supplemental Material

<http://genesdev.cshlp.org/content/suppl/2013/05/06/27.9.1059.DC1>
<http://genesdev.cshlp.org/content/suppl/2013/05/13/27.9.1059.DC3>

Related Content

Dynamic binding of RBPJ is determined by Notch signaling status
David Castel, Philippos Mourikis, Stefanie J.J. Bartels, et al.
[Genes Dev. June , 2013 27: 1313](#)

References

This article cites 42 articles, 14 of which can be accessed free at:
<http://genesdev.cshlp.org/content/27/9/1059.full.html#ref-list-1>

Articles cited in:

<http://genesdev.cshlp.org/content/27/9/1059.full.html#related-urls>

License

Email Alerting Service

Receive free email alerts when new articles cite this article - sign up in the box at the top right corner of the article or [click here](#).

Use CRISPRmod for targeted modulation of endogenous gene expression to validate siRNA data

horizon
a PerkinElmer company